Scaling properties of self-organized criticality

P. A. Robinson
School of Physics, University of Sydney, New South Wales 2006, Australia
(Received 8 June 1993)

The scaling properties of a sandpile-type system which displays self-organized criticality are investigated analytically and numerically in two and three dimensions. An earlier clump-based analytical model is modified and extended to account for the scalings and probability distributions of avalanche size, radius, duration, and maximum power in this system, and the scalings of the avalanche sizes with parameters of the driving and system size are also investigated in detail. Comparison with numerical results shows that this model can account for the probability distributions and scaling exponents of both scalar and vector fields in two and three dimensions, once one basic exponent has been determined numerically or by other means.

PACS number(s): 05.50.+q, 05.70.Jk

I. INTRODUCTION

Sandpile-type models of self-organized criticality (SOC) have been studied extensively since their introduction by Bak *et al.* [1]. These models display a unique critical state in which a statistical balance is reached between driving and relaxation via avalanches and in which power-law correlations in space and time are observed.

The key properties of the SOC state are the scaling exponents of various measurable quantities. These exponents have been studied in a variety of sandpile-type models by analytic means, and using numerical simulations based on cellular automatons [1–14]. In particular, Zhang [4] developed a simple analytic model which was able to explain a number of the observed exponents, while Hwa and Kardar [6] used renormalization group theory to make similar estimates for a related continuum model. Exponents for the scaling of rms field components in vector-field SOC were also recently derived [14]. In general, the exponents derived for the various models differ from one another, implying that they are in different universality classes.

In this paper we modify and extend Zhang's [4] theory to treat scalar- and vector-field SOC using a model introduced in a previous work [14]. The focus of that work was on the effects of vector fields and random driving on the properties of the SOC state, and numerical work was restricted to two-dimensional systems. Here, our emphasis is on generalizing previous clump-based models [4,14] to calculate the probability distributions and scaling exponents for avalanche size, radius, duration, and peak power dissipation, and for rms vector-field components. Extensive comparison here with numerical results in two and three dimensions shows that the resulting clump-based theory can account for all the observed exponents, once one basic exponent has been determined numerically or by other means. This work thus extends and further verifies the clump-based analysis.

II. THE MODEL

The model used here [14] involves a D-component vector field $\mathbf{h}$ defined on a two- or three-dimensional rectangular grid of side N. The driving step consists of adding a field increment (analogous to a sand grain) $\mathbf{g}$ to a randomly chosen site, with

$$\mathbf{h} \rightarrow \mathbf{h} + \mathbf{g}, \tag{1}$$

at that site. The increment $\mathbf{g}$ is a random variable, with the means of its components satisfying

$$\langle g_n \rangle = \begin{cases} \mu, & n = 1 \\ 0, & n > 1 \end{cases} \tag{2}$$

at every site. Each component of $\mathbf{g}$ also has an additive random part uniformly distributed between $-\Delta$ and Δ. The choice of g_1 to be the only component with a nonzero mean involves no loss of generality because the coordinates defining the field components can always be rotated to bring $\langle \mathbf{g} \rangle$ into the form given by (2).

Relaxation occurs when the addition of a grain causes $h = |\mathbf{h}|$ to exceed a critical value, which we set equal to unity without loss of generality. The field at the unstable site then relaxes to zero, with its original value being equally distributed to its $2d$ nearest neighbors, where d is the dimensionality of the system, thereby conserving $\mathbf{h}$ in this step. Some of these neighbors may then become unstable and relax in turn (with all unstable sites relaxing simultaneously), followed by relaxations of more distant sites. Relaxation is allowed to proceed until all sites are stable before the next field increment is added.

The (open) boundary condition used is that $\mathbf{h} = \mathbf{0}$ for all sites on the edge of the grid. In the case of a sandpile, for example, this implies that grains that reach the edge fall off and leave the pile, thereby enabling a statistically steady state to be attained.

In our model, the size s of the avalanche is defined to

be the total number of different sites to undergo relaxation, while the activation number a is the total number of relaxations, accounting for multiple relaxations at a given site (some authors call a the size). The duration t of the avalanche is the total number of iterations required for the system to become stable once an avalanche starts. We define the radius r to be

$$r = r_0 + \frac{1}{2d}\sum_{n=1}^{d}[\max(R_n) - \min(R_n)], \tag{3}$$

where the maximums and minimums are taken over all sites (at locations $\mathbf{R}$) that are active during the avalanche, $r_0 = \pi^{-1/2}$ in two dimensions (2D), and $r_0 = (3/4\pi)^{1/3}$ in three dimensions (3D). This definition uses the "taxicab" metric for computational speed, coincides with the usual Euclidean radius if the avalanche is spherical, but is only approximately $(2d)^{-1}$ times the chain length for a straight linear chain. Note that the value of r_0 is chosen to give a single-site avalanche a radius equal to that of a d sphere of unit volume. The maximum power p (a quantity of interest in some astrophysical applications [12], for example) is defined to be equal to the maximum number of sites simultaneously active during the avalanche.

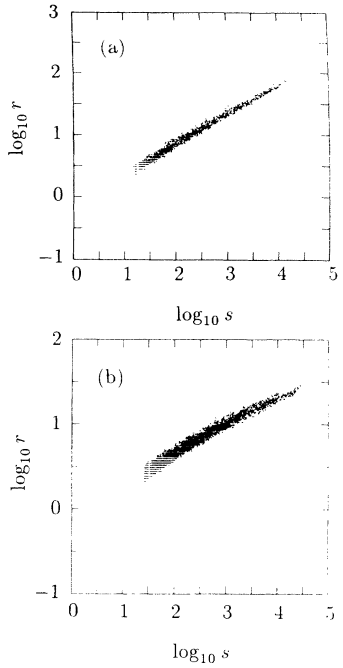

FIG. 1. Scatter plots of r vs s for (a) $d = 2$, $D = 1$, $N = 200$, $\mu = 0.16$, and $\Delta = 0.4$; (b) $d = 3$, $D = 1$, $N = 80$, $\mu = 0.32$, and $\Delta = 0.4$.

III. THEORY AND NUMERICAL RESULTS

In this section we explore the scaling properties of scalar SOC, followed by a brief discussion of the vector case. Both two- and three-dimensional systems are investigated, with the theory being developed and numerically verified in parallel. We restrict attention to $\Delta^2/\mu < 100$ throughout, in accord with Robinson's work [14], which found that SOC breaks down for $\Delta^2/\mu \gg 100$.

A. Scalings with avalanche size

After addition of a large number of field increments, a system defined by the above model settles into a statistically steady SOC state. Zhang [4] proposed a theory of this state for a related model, using an approximation to the behavior of individual avalanche clusters. In his theory he assumed that the avalanches are d-dimensional compact objects (possibly with rough boundaries, although this effect was not considered in detail). Because a site that has just been activated is less likely than average to reactivate on the next step, he introduced an effective repulsive potential between recently active sites, which have density $\rho = t/s$, by analogy with the theory of self-avoiding walks [15,16]. This led to the scalings

$$r \sim s^{1/d}, \tag{4}$$

$$t \sim r^{(2+d)/3} \sim s^{(2+d)/3d}, \tag{5}$$

$$\rho \sim r^{2(1-d)/3}. \tag{6}$$

Figures 1(a) and 1(b) show scatter plots of r vs s in 2D and 3D systems, respectively, for the present model. The lower boundary of the occupied region in Fig. 1(a) corresponds very closely to the (taxicab) radius $r_{\min} \approx r_0 s^{1/d}$ of the *most compact* cluster of the relevant size (i.e., a sphere for large r), and there is only a factor of $\lesssim 2$ scatter above this curve, decreasing slightly at large s. This evidence strongly supports Zhang's contention that the avalanche clusters are compact and two dimensional in this case. The corresponding 3D situation is shown in Fig. 1(b): at small s the data are scattered between the radius of the most compact cluster possible and the absolute upper bound $r = r_0 + (s-1)/2d$ for a connected cluster. At larger s the data points are scattered within a factor of ~ 2 of the lower bound, with somewhat greater spread than in 2D. This indicates that the clusters have more diffuse boundaries than in 2D, but that their dimensionality remains close to d. Upon introducing the notation $Q \sim s^{\delta_Q}$ for the scaling of an arbitrary quantity Q with s, the numerical scalings extracted from Figs. 1(a) and 1(b) are $\delta_r = 0.50 \pm 0.01$ in 2D and $\delta_r = 0.34 \pm 0.04$ in 3D, in good agreement with (4).

Figure 2 comprises scatter plots of t vs s in 2D and 3D systems for the same parameters used in Fig. 1, with t satisfying the inequalities

$$\max(r_{\min}, 1) \le t \le s. \tag{7}$$

The data points generally lie well clear of both bounds for $s \gtrsim 20$. In this range Fig. 2 yields $\delta_t = 0.64 \pm 0.03$ in 2D and $\delta_t = 0.52 \pm 0.03$ in 3D, in reasonable agreement with (5). These values also agree with earlier results for related models [2,3].

The increase in the total activation number a with time has two parts: new sites are activated at the boundary

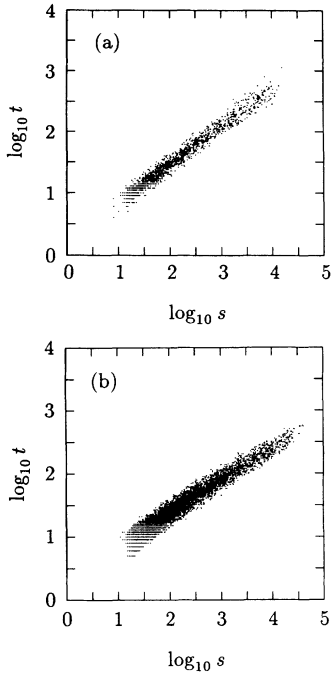

FIG. 2. Scatter plots of t vs s for the same parameters as Fig. 1. (a) $d = 2$. (b) $d = 3$.

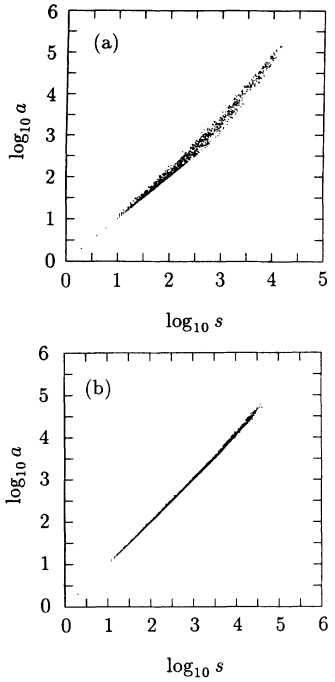

FIG. 3. Scatter plots of a vs s for the same parameters as Fig. 1. (a) $d = 2$. (b) $d = 3$.

of the avalanche as s increases, and old sites reactivate within the avalanche cluster. If we extend Zhang's theory by assuming a uniform density ρ' of active sites within an avalanche cluster, we find

$$\frac{ds}{dt} = A_d \rho' \frac{\partial s}{\partial r}, \tag{8}$$

$$\frac{da}{dt} = A_d \rho' \frac{\partial s}{\partial r} + \rho' s, \tag{9}$$

where A_d is a d-dependent constant and the $\partial s/\partial r$ terms describe expansion of the cluster boundary. Equations (5), (6), and (8) yield

$$\rho' \sim s^{(1-d)/3d} \sim \rho^{1/2}. \tag{10}$$

Similarly, taking the ratio of (9) to (8) and integrating with respect to s, we predict

$$a \approx s, \quad s \text{ small} \tag{11}$$

$$a \sim s^{(d+1)/d}, \quad s \text{ large}. \tag{12}$$

Robinson [14] found $a \approx s$ for $s \lesssim 100$, and $\delta_a = 1.52 \pm 0.10$ for $s \gtrsim 300$ in 2D [see Fig. 3(c)], in agreement with (11) and (12). Likewise, the scatter plot in Fig. 3(b) yields $a \approx s$ for $s \lesssim 10^3$ and $\delta_a = 1.27 \pm 0.07$ for $s \gtrsim 10^4$, also in good accord with theory. The crossover points $s = s_c$ between the large- and small-s regimes in (11) and (12) occur for $A_d \partial s/\partial r \approx s$. Inserting $s_c = 300$ and $s_c = 5000$ for the 2D and 3D crossover points, we find $A_2 \approx 5$ and $A_3 \approx 3.5$, with $r \approx 8$ and $r \approx 10$, respectively. This implies that active sites at the edges of the cluster are three to five times more likely to activate their nearest neighbors than are active sites in the interior. This result is intuitively reasonable, because recently activated sites are less likely to be near instability than sites immediately outside the growing cluster. The disparity is actually even larger than these numbers indicate, given that boundary sites actually have at least one interior site among their neighbors (for $s > 1$). Our picture is thus that a increases almost entirely due to the expansion of the cluster until, at the crossover point, reactivations within the cluster begin to dominate.

The maximum power is a useful quantity measured in some applications [12]. Our definition (see Sec. II) implies that the power dissipation is proportional to the right hand side of (9). Hence, the peak power p scales as

$$p \sim \begin{cases} s^{2(d-1)/3d}, & s < s_c \end{cases} \tag{13}$$

$$\begin{cases} s^{(2d+1)/3d}, & s_c < s. \end{cases} \tag{14}$$

Figures 4(a) and 4(b) show scatter plots of p vs s in 2D and 3D, respectively. As expected from the theory, breakpoints in Figs. 4(a) and 4(b) are seen at the same values of s_c as in Fig. 3. For large s these data yield $\delta_p = 0.91 \pm 0.10$ and $\delta_p = 0.75 \pm 0.10$ in 2D and 3D, respectively, in good agreement with the theory. For small s, the corresponding values are 0.43 ± 0.02 and 0.48 ± 0.03, respectively, both of which are somewhat higher than predicted by theory, particularly in 2D. This may indicate that the small-s regime is not unequivocally reached or that the present form of the surface-area terms in (8) and (9) requires some modification.

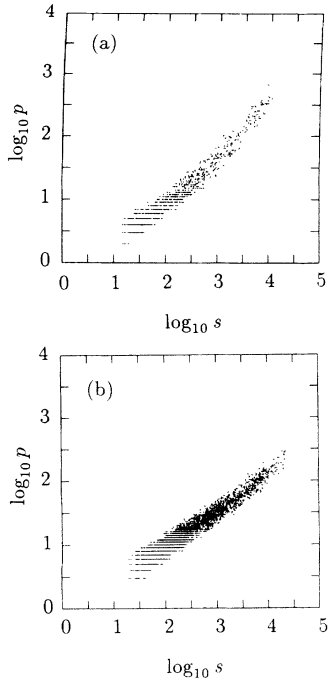

FIG. 4. Scatter plots of p vs s for the same parameters as Fig. 1. (a) $d = 2$. (b) $d = 3$.

B. Probability distributions

In the SOC state the probability distribution $D(s)$ of s scales as

$$D(s) \sim s^{1-\tau}. \tag{15}$$

Robinson [14] found $\tau = 2.23 \pm 0.05$ for $d = 2$ and $D = 1$, in agreement with earlier results for a related model [7]. Figure 5 shows $D(s)$ vs s for $d = 3$ and $D = 1$ with $N = 80$, $\mu = 0.32$, and $\Delta = 0.4$. These data yield $\tau = 2.35 \pm 0.05$ for $10^{0.5} \lesssim s \lesssim 10^4$. Zhang and coworkers [4,13] argued for $\tau = 3 - 2/d$ by noting that the mean time-averaged transport current density j leaving a given point scales as r^{1-d}, where r is the distance from that point. This value of τ accords with the $d = 3$ results obtained here, but disagrees unequivocally with the $d = 2$ value. A justification for this disagreement can be seen by examining Zhang's argument in more detail. Generalizing his argument slightly, he essentially showed that j can be written as

$$j = -\frac{d}{dr} \int_0^\infty D(r') F(r, r') dr', \tag{16}$$

where $F(r, r')$ is the mean local transport at a radius r due to an avalanche of radius r'. By making the step-function approximation $F(r, r') = \theta(r' - r)$ he obtained $j \propto D(r) \propto r^{1-d}$ and then, using $s \sim r^d$, $\tau = 3 - 2/d$. Unfortunately, this approximation is only fully justified for avalanche clusters that can be modeled by d-spheres with sharp edges. In general it is not possible to calculate τ from (16) without knowing the detailed structure of $F(r, r')$. Significantly, Zhang's argument would seem to imply a single universality class for sandpile models, whereas several have actually been observed [5,7,10]. Hence, we conclude that the structure of $F(r, r')$ can indeed be important. In what follows we use our numerically determined values of τ as inputs to the remainder of the theory; alternatively, a dynamical renormalization group calculation could be used to calculate τ from first principles (e.g., [6]).

Once the scaling of a quantity Q with s is known the scaling of the distribution $D(Q)$ with Q can immediately be written as

$$D(Q) \sim Q^{1-\alpha_Q}, \tag{17}$$

with

$$\alpha_Q = 2 + (\tau - 2)/\delta_Q. \tag{18}$$

Figures 6–9 show the distributions of r, t, a, and p,

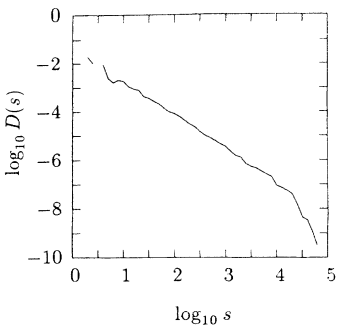

FIG. 5. Probability distribution $D(s)$ vs s for $d = 3$, $D = 1$, $N = 80$, $\mu = 0.32$, and $\Delta = 0.4$.

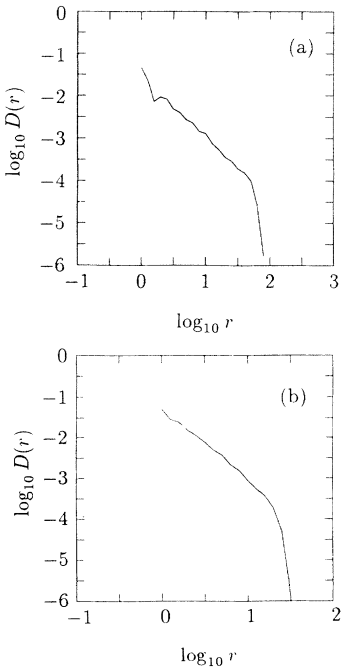

FIG. 6. Probability distribution $D(r)$ vs r for (a) $d = 2$, $D = 1$, $N = 200$, $\mu = 0.16$, and $\Delta = 0.4$; (b) $d = 3$, $D = 1$, $N = 80$, $\mu = 0.32$, and $\Delta = 0.4$.

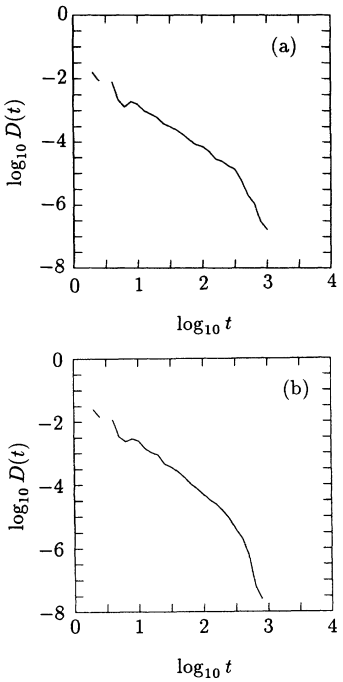

FIG. 7. Probability distribution $D(t)$ vs t for the same parameters as Fig. 6. (a) $d = 2$. (b) $d = 3$.

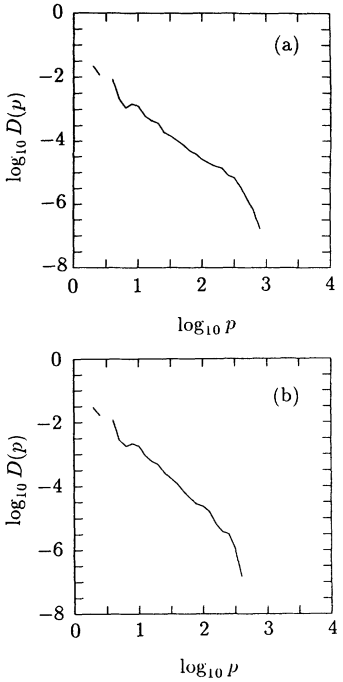

FIG. 9. Probability distribution $D(p)$ vs p for the same parameters as Fig. 6. (a) $d = 2$. (b) $d = 3$.

respectively, in 2D [(a) frames] and 3D [(b) frames]. The results in Fig. 6 yield $\alpha_\tau = 2.44 \pm 0.05$ and $\alpha_\tau = 2.8 \pm 0.1$ in 2D and 3D, respectively. The 2D result is in excellent agreement with the value of 2.46 ± 0.10 obtained from (18) using our numerical value of τ. The 3D value is significantly lower than the corresponding estimate of 3.05 ± 0.15 obtained using τ; however, the range of the power law is only one order of magnitude in this case, making the fit less convincing. Simulations with larger systems ($N \approx 200$) would be necessary to resolve this point conclusively.

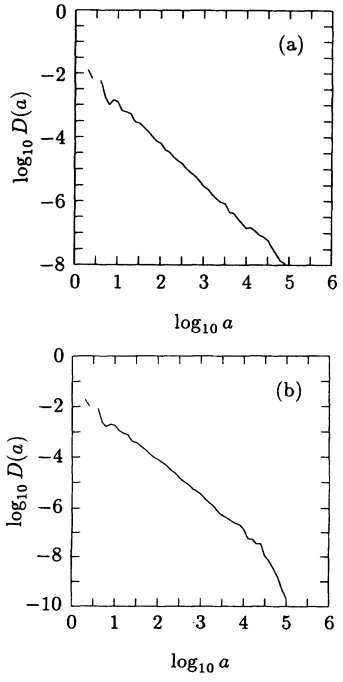

FIG. 8. Probability distribution $D(a)$ vs a for the same parameters as Fig. 6. (a) $d = 2$. (b) $d = 3$.

Figure 7 yields $\alpha_t = 2.36 \pm 0.05$ and $\alpha_t = 2.62 \pm 0.10$, in 2D and 3D, respectively, in good agreement with the corresponding estimates (from the numerical value of τ) of 2.35 ± 0.04 and 2.68 ± 0.09.

For $s < s_c$ (the value of a corresponding to s_c can be read off Fig. 3) Fig. 8 gives $\alpha_a = 2.25 \pm 0.05$ and $\alpha_a = 2.35 \pm 0.05$ in 2D and 3D, respectively, in excellent agreement with the prediction $\alpha_a = \tau$ in this regime. There is insufficient range available with $s > s_c$ to estimate α_a in the latter regime — scatter plots such as Fig. 3 give more useful results at large a because they do not require such good statistics to yield the relevant exponent.

For $s < s_c$ Fig. 9 implies $\alpha_p = 2.61 \pm 0.10$ and $\alpha_p = 2.82 \pm 0.05$ in 2D and 3D, respectively. These values agree well with the theoretical predictions (using the numerically determined value of τ) of 2.69 ± 0.15 and 2.79 ± 0.11, respectively. However, as with Fig. 8, there is too little range available to obtain an accurate value of α_p from Fig. 9 for $s > s_c$.

C. Scalings with system size and driving parameters

We now turn to examine the scaling of the means (over all increments added) of s and a with N, μ, and Δ. The scalings with μ and Δ do not appear to have been previously investigated for any model, certainly not for the

present one. The scaling of $\langle s \rangle$ with N can be estimated by noting that $\langle s \rangle$ is given by

$$\langle s \rangle = \int_1^{N^d} sD(s)ds \Big/ \int_1^{N^d} D(s)ds. \tag{19}$$

The finite-size cutoff in $D(s)$ is a purely geometric effect. For compact avalanches of dimension d this cutoff thus occurs at $s \sim N^d$ and, hence,

$$\langle s \rangle \sim N^{d(3-\tau)}, \tag{20}$$

for $2 < \tau < 3$. Using the above-determined values of τ, we predict exponents of 1.54 ± 0.10 and 1.95 ± 0.15, in 2D and 3D, respectively, consistent with the numerical results shown in Fig. 10, which yield

$$\langle s \rangle \sim N^{1.45 \pm 0.06}, \tag{21}$$

$$\langle s \rangle \sim N^{2.01 \pm 0.05}, \tag{22}$$

respectively, where the errors here and below are from least-squares fits. The mean size $\langle s \rangle$ thus increases more slowly than the system size N^d for $d = 2, 3$. Note that for $\langle s \rangle \lesssim 20$ in 2D the slope of the $\langle s \rangle$ vs N plot changes because of the restriction $\langle s \rangle \leq \langle a \rangle$ (see next paragraph); in 3D the corresponding change is too small to be discernable from Fig. 10.

The scaling $\langle a \rangle \propto N^2$ was determined by Kadanoff *et al.* [5] and Tang and Bak [3], who argued that transport proceeds diffusively, so that the mean number of relaxations required to transport a unit field increment to the boundary must scale as N^2. Numerically, we find

$$\langle a \rangle \sim N^{1.995 \pm 0.004}, \tag{23}$$

$$\langle a \rangle \sim N^{2.04 \pm 0.04} \tag{24}$$

in the present model in 2D and 3D, respectively, in agreement with the theoretical prediction. The resulting scaling

$$\langle s \rangle \sim \langle a \rangle^{d(3-\tau)/2}, \tag{25}$$

together with the requirement $\langle s \rangle \leq \langle a \rangle$, implies $\tau \geq 3 - 2/d$ for large N, which is satisfied by the values of τ found above.

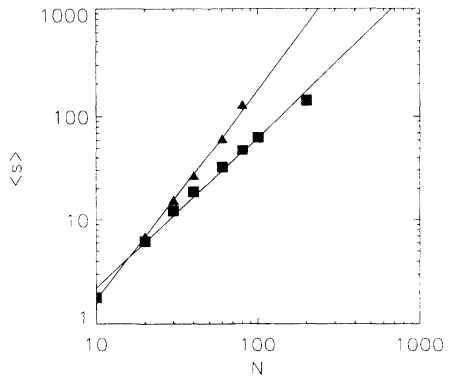

FIG. 10. Dependence of $\langle s \rangle$ on N for $d = 2$ (squares) and $d = 3$ (triangles). Parameters other than N are the same as in Fig. 1. Solid lines are least-squares lines of best fit.

Interestingly, if we calculate the mean of a from the power-law part of $D(a)$ and require $\langle a \rangle \sim N^2$ we obtain $\alpha_a = 3 - 2/(d+1)$, which is inconsistent with the numerical values obtained from Fig. 8. Thus it appears that the power-law part of $D(a)$ alone cannot be used to calculate the scaling of $\langle a \rangle$ with N. The reason is that the averages of a and s depend most strongly on the large-a and large-s parts of the probability distributions, respectively. Unlike s (which satisfies $\leq N^d$), a does not have an absolute upper bound and so is more sensitive to details of the behavior of $D(a)$ at large a.

Theoretically, we expect

$$\langle a \rangle \sim \mu, \tag{26}$$

because (i) the mean outward rate of transport across the boundaries must equal the mean input rate, which is proportional to μ, (ii) the outward transport rate is proportional to the number of activations on the boundaries, because each such activation transfers field across the boundary, and (iii) the number of activations at the boundaries is proportional to the total number of activations, averaged over all locations of the initially unstable site. The scalings of $\langle a \rangle$ and $\langle s \rangle$ with μ in 2D and 3D are shown in Figs. 11(a) and 11(b), respectively. In 2D, numerical values of the exponents for $\langle s \rangle$ and $\langle a \rangle$ vs μ are

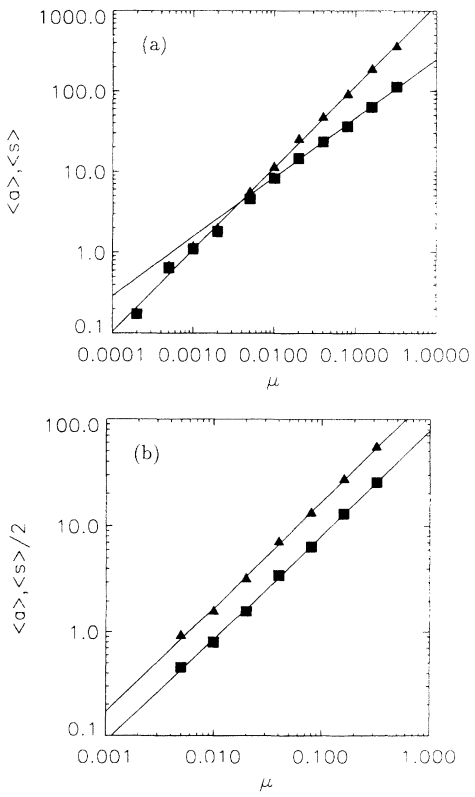

FIG. 11. Dependence of $\langle s \rangle$ (squares) and $\langle a \rangle$ (triangles) on μ. Parameters other than μ are the same as in Fig. 1. Solid lines are least-squares lines of best fit. (a) $d = 2$ with $\langle s \rangle$ fitted for $\mu > 0.01$. (b) $d = 3$ with the $\langle s \rangle$ data offset downward by a factor of 2 for clarity.

0.73 ± 0.03 and 1.014 ± 0.015, respectively, in excellent agreement with (25) and (26) using our numerical value of τ. Likewise, the respective 3D exponents of 0.98 ± 0.03 and 1.00 ± 0.04 are in good agreement with theory.

The scalings of $\langle s \rangle$ with $\langle a \rangle$ in 2D and 3D are shown in Figs. 12(a) and 12(b), respectively. For large $\langle s \rangle$ in 2D we find an exponent of 0.76 ± 0.02, numerically, in agreement with (25). For small $\langle s \rangle$ the exponent is 0.973 ± 0.008 in 2D, slightly below the theoretical value of 1, but probably underestimated because of the proximity of the breakpoint in the behavior of $\langle s \rangle$ and the relatively small range of the fit. In 3D an exponent of 0.985 ± 0.002 is found, fitted over the entire range shown, with no discernable breakpoint. This compares well with the theoretical values of 1 and 0.975 ± 0.075 at small and large $\langle a \rangle$, respectively.

The mean net rate of addition of field increments to the system is independent of Δ, the randomness in the driving. Hence, we predict that $\langle a \rangle$ and $\langle s \rangle$ should be independent of Δ. This prediction is found to be borne out by our numerical results for all values of Δ sufficiently small that SOC is not significantly modified or destroyed [14].

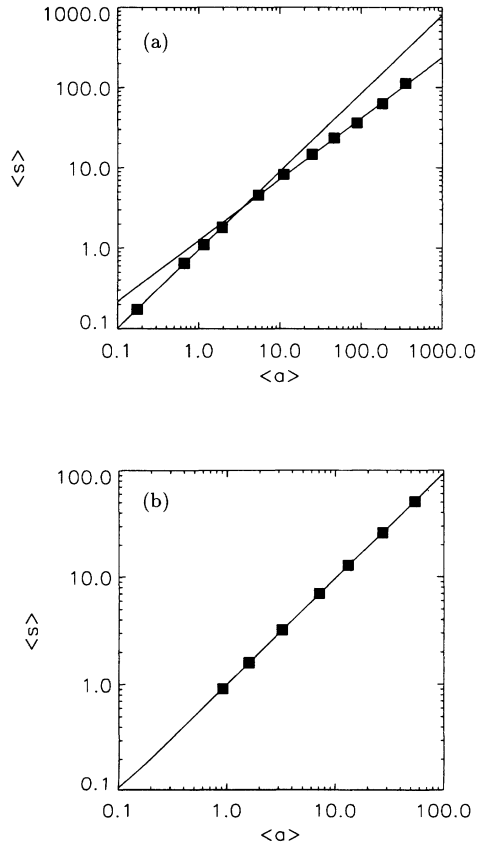

FIG. 12. Dependence of $\langle s \rangle$ on $\langle a \rangle$ from Figs. 11(a) and 11(b). Solid lines are least-squares lines of best fit. (a) $d = 2$, with upper and lower fits for $\langle a \rangle > 10$ and $\langle a \rangle < 3$, respectively. (b) $d = 3$; with a single line of best fit.

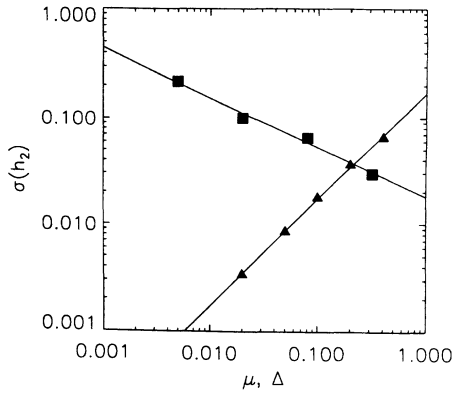

FIG. 13. Dependence of $\sigma(h_2)$ on Δ (triangles) and μ (squares) in 3D with $D = 2$ and $N = 40$. The value of μ is fixed at 0.08 when determining the Δ dependence, while $\Delta = 0.4$ is fixed for the μ dependence. Solid lines are least-squares lines of best fit.

D. Vector-field scalings

We now consider the scaling of the variance of the component h_2 for a vector field with $D = 2$ as a function of μ and Δ. Robinson [14] found that the component h_1, driven with nonzero mean increment, dominates the evolution of the system, except for $\Delta^2 \gtrsim 300\mu$, with the other components slaved to it. By balancing the rate of input of the variance $\sigma^2(h_2)$ against its loss across the boundary he derived the scaling

$$\sigma^2(h_2) \sim \Delta^2/\mu. \tag{27}$$

Numerically, he found

$$\sigma^2(h_2) \sim \frac{\Delta^{1.98\pm0.02}}{\mu^{1.01\pm0.03}}, \tag{28}$$

for the present model in 2D, in good agreement with (27). The corresponding results in 3D are presented in Fig. 13 for $D = 2$ and $N = 40$. We find

$$\sigma^2(h_2) \sim \frac{\Delta^{2.00\pm0.03}}{\mu^{0.93\pm0.07}}, \tag{29}$$

also in good agreement with (27).

IV. SUMMARY AND DISCUSSION

The scaling properties and probability distributions of scalar and vector sandpile models have been investigated in two and three dimensions in this work. Scaling exponents and probability distributions for avalanche size, activation number, radius, duration, and peak power have been derived in terms of one basic exponent τ by modifying and extending Zhang's [4] model to incorporate the density of active sites. This generalization, and the extension of the numerical results to three dimensions when verifying the theory, are the key results of the present work.

Extensive comparison with numerical results in 2D and 3D has yielded good agreement between theory and simulation for a wide range of exponents, thereby confirming the internal consistency of the clump-based model for SOC and providing extensive confirmation of the values of τ. Significantly, in two dimensions, the value $\tau = 2.23 \pm 0.05$ is inconsistent with Zhang's estimate $\tau = 2$. A reason for this discrepancy is suggested and it is noted that Zhang's original argument would have implied only a single universality class for sandpile SOC in two dimensions, contrary to numerical results from other authors.

The scalings of average avalanche size and activation number have been investigated as functions of the system size and the driving parameters. Again, good accord between theory and numerical results is found. Vector-field scalings in 3D are also found to conform with Robinson's earlier theory [14], previously confirmed only in the 2D case.

ACKNOWLEDGMENTS

The author thanks A. Melatos for his comments on the draft of this paper. This work was supported by the Australian Research Council.

[1] P. Bak, C. Tang, and K. Wiesenfeld, Phys. Rev. Lett. **59**, 381 (1987).
[2] P. Bak, C. Tang, and K. Wiesenfeld, Phys. Rev. A **38**, 364 (1988).
[3] C. Tang and P. Bak, Phys. Rev. Lett. **60**, 2347 (1988).
[4] Y.-C. Zhang, Phys. Rev. Lett. **63**, 470 (1989).
[5] L. P. Kadanoff, S. R. Nagel, L. Wu, and S.-M. Zhou, Phys. Rev. A **39**, 6524 (1989).
[6] T. Hwa and M. Kardar, Phys. Rev. Lett. **62**, 1813 (1989).
[7] S. S. Manna, J. Stat. Phys. **59**, 509 (1990).
[8] D. Dhar, Phys. Rev. Lett. **64**, 1613 (1990).
[9] K. O'Brien, L. Wu, and S. R. Nagel, Phys. Rev. A **43**, 2052 (1991).
[10] K. Christensen, H. C. Fogedby, and H. J. Jensen, J. Stat. Phys. **63**, 653 (1991).
[11] S. N. Majumdar and D. Dhar, J. Phys. A **24**, L357 (1991).
[12] E. T. Lu and R. J. Hamilton, Astrophys. J. **380**, L89 (1991).
[13] L. Pietronero, P. Tartaglia, and Y.-C. Zhang, Physica A **173**, 22 (1991).
[14] P. A. Robinson, Phys. Rev. E **49**, 1984 (1994).
[15] L. Pietronero, Phys. Rev. B **27**, 5887 (1983).
[16] D. J. Amit, G. Parisi, and L. Peliti, Phys. Rev. B **27**, 1635 (1983).